ADVANCED FUNCTIONAL MATERIALS
www.afm-journal.de

Nitridation and Layered Assembly of Hollow TiO_2 Shells for Electrochemical Energy Storage

*Geon Dae Moon, Ji Bong Joo, Michael Dahl, Heejung Jung, and Yadong Yin**

The nitridation of hollow TiO_2 nanoshells and their layered assembly into electrodes for electrochemical energy storage are reported. The nitridated hollow shells are prepared by annealing TiO_2 shells, produced initially using a sol–gel process, under an NH_3 environment at different temperatures ranging from 700 to 900 °C, then assembled to form a robust monolayer film on a water surface through a quick and simple assembly process without any surface modification to the samples. This approach facilitates supercapacitor cell design by simplifying the electrochemical electrode structure by removing the need to use any organic binder or carbon-based conducting materials. The areal capacitance of the as-prepared electrode is observed to be ≈180 times greater than that of a bare TiO_2 electrode, mainly due to the enhanced electrical conductivity of the TiN phase produced through the nitridation process. Furthermore, the electrochemical capacitance can be enhanced linearly by constructing an electrode with multilayered shell films through a repeated transfer process (0.8 to 7.1 mF cm^{-2}, from one monolayer to 9 layers). Additionally, the high electrical conductivity of the shell film makes it an excellent scaffold for supporting other psuedocapacitive materials (e.g., MnO_2), producing composite electrodes with a specific capacitance of 743.9 F g^{-1} at a scan rate of 10 mV s^{-1} (based on the mass of MnO_2) and a good cyclic stability up to 1000 cycles.

1. Introduction

Titanium dioxide (TiO_2) is a widely used material across various applications including pigments, due to its brightness and high refractive index, UV light absorbers, in electronics for memristors, and in solar energy conversion.[1] TiO_2, especially in the anatase form, has been studied vigorously as a photocatalyst under ultraviolet or visible light by exploiting metal/non-metal doping, which is useful in environmental purification and water splitting.[2] TiO_2 has also attracted much interest in the field of energy storage, including lithium ion batteries and supercapacitors.[3] Despite its relatively low theoretical capacity (≈330 mAh g^{-1}) compared to graphite (≈372 mAh g^{-1}), TiO_2 has been widely investigated as an anode material in lithium rechargeable batteries because of its low volume change (<4%) during Li-ion insertion/desertion, which is directly related to stability or cycling performance.[4] For electrochemical capacitors, mesoporous TiO_2 films showed considerably enhanced electrochemical properties when $LiClO_4$ was used as an electrolyte in propylene carbonate (PC).[5] Well-ordered TiO_2 nanotube arrays hold good potential as supercapacitor electrodes because they are chemically stable and have open-ended structures rendering an extremely large and solvated ion accessible surface area. Nevertheless, the reported specific capacitances of TiO_2 nanotube arrays (<1 mF cm^{-2}) are not comparable to those of other metal oxides including RuO_2, MnO_2, and Co_3O_4.[6] The small specific capacitance of TiO_2 can be attributed to low electronic conductivity and poor electrochemical activity.[7] It was found that the reduction of Ti^{4+} to Ti^{3+} with oxygen depletion of the TiO_2 can increase the capacitance properties by making TiO_2 more conductive in a charging process.[6b] Recently, it was found that hydrogenation can improve the electrochemical performance of TiO_2 nanotube arrays up to 3.24 mF cm^{-2} due to the increased donor density and the improved density of surface hydroxyl groups, which are characteristics of electronic conductivity and electrochemical activity, respectively.[8]

It is well known that TiO_2 only contributes a low non-faradic and faradic capacitance in terms of charging mechanism.[9] Generally, TiO_2 capacitors behave as conventional electric double layer capacitors (EDLC) rather than pseudocapacitors like other metal oxides. It is believed that pure titania shows very low electrochemical capacitance (<40 μF cm^{-2}) due to its high electrical resistance and low faradic capacitance. In addition to efforts to improve the electrical conductivity through the introduction of oxygen deficiencies in TiO_2 structures, titanium nitride (TiN) nanotube arrays[10,11] and microspheres/nanoparticles[12,13] were also investigated since TiN has a high electronic conductivity (≈10^5 S m^{-1}, bulk). However, the properties of TiN nanotube arrays are limited to a fixed dimension on the substrate in electrochemical cells because Ti foil is commonly

Dr. G. D. Moon, Dr. J. B. Joo, M. Dahl, Prof. Y. Yin
Department of Chemistry
University of California
Riverside, CA, 92501, USA
E-mail: yadong.yin@ucr.edu
Prof. H. Jung
Department of Mechanical Engineering
University of California
Riverside, CA, 92521, USA

DOI: 10.1002/adfm.201301718

used as a substrate and the subsequent structure will go through an oxidation process. This limitation makes it hard to fabricate large-sized electrochemical cells, which creates further difficulty for tuning the supercapacitor properties. In the case of TiN spheres, the use of other conducting materials (e.g. activated carbon) and polymer binders (e.g. polyvinylidene fluoride (PVDF)) is unavoidable due to the difficulties of fabricating an electrode without them.

Herein, we report the successful synthesis of hollow nitridated titania shells on a sub-micrometer scale through simple nitridation of sol-gel derived hollow TiO_2 spheres under ammonia environment at elevated temperatures. The nitridation process is facilitated by the thermal decomposition of NH_3 to H_2 and N_2 at high temperatures.[14] These nitridated hollow shells are assembled into a monolayer film on a water surface, enabling subsequent transfer onto a substrate, which can be done repeatedly and on a large scale. We demonstrate that these films of nitridated shells, assembled without the need of any binder materials, show a great enhancement in electrochemical performance compared to the TiO_2 sphere films. Additionally, the areal capacitance of a nitridated shell electrode shows a linear increase with the layer number. Furthermore, the deposition of MnO_2 on the surface of a nitridated film causes a remarkable improvement in the specific capacitance due to the interplay of the high electronic conductivity of TiN phase (formed during nitridation) and the high electrochemical activity of MnO_2. The composite film supercapacitor displays great cyclic stability up to 1000 cycles as determined by cyclic voltammetry tests.

2. Results and Discussion

The synthesis of hollow TiO_2 spheres follows a procedure previously reported by our group.[15] After etching the core SiO_2 by a NaOH solution and neutralizing by a HCl solution, amorphous hollow spheres with a shell thickness of 30–40 nm could be obtained, which could be made crystalline with a predominantly anatase phase through calcination in static air at 800 °C without any morphological change (**Figure 1**). The crystallized hollow TiO_2 spheres can be further transformed into nitride shells without losing their hollow structure by annealing at different temperatures under ammonia gas flow. After nitridation, the color of the powder turned from the original white to green or black depending on the nitridation temperature. **Figure 2** shows the X-ray diffraction spectra of the TiO_2 calcined at 800 °C and the samples nitridated at different temperatures. The spectrum of TiO_2 mostly corresponds to anatase TiO_2 (JC-PDS, #73-1764) except for a small portion of rutile phase, indicated by an asterisk. After nitridation under NH_3 atmosphere, all the peaks for anatase TiO_2 disappear while peaks indicating the cubic structure of TiN are formed with a small peak for rutile phase TiO_2 remaining (JC-PDS, #87-0633). The conversion from anatase TiO_2 to cubic TiN can be near completion if annealed under ammonia above 800 °C.

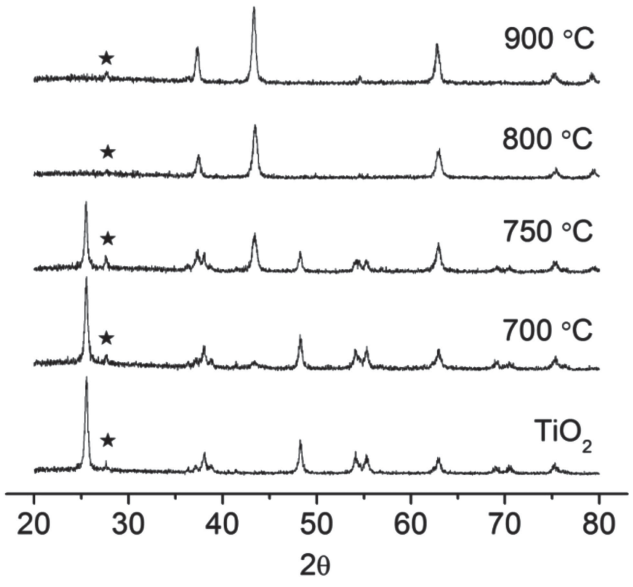

Figure 2. XRD spectra of hollow TiO_2 sphere and nitridated shell samples treated at different temperatures. Rutile phase is indicated by asterisks.

We also performed X-ray photoelectron spectroscopy (XPS) measurements to examine the effect of nitridation on the chemical composition and oxidation state of the hollow TiO_2 spheres (**Figure 3**a). The two principal peaks located at ≈459 and ≈465 eV (dotted line) correspond to the characteristic Ti $2p_{3/2}$ and $2p_{1/2}$ of Ti^{4+}.[16] The peak for In 3d originated from the substrate (ITO glass). The upper spectrum in Figure 3a shows a clear signal for nitrogen (≈396 eV, N 1s) appearing in the nitridated sample at 900 °C while there are no such peaks in the TiO_2 sample (lower spectrum). Furthermore, the peaks of the nitridated shell sample are shifted toward a lower binding energy, which can be assigned to be multiple peaks corresponding to Ti–O ($2p_{3/2} \approx 459$ and $2p_{1/2} \approx 465$ eV), Ti–N ($2p_{3/2} \approx 456$ and $2p_{1/2} \approx 462$ eV), and Ti–N–O ($2p_{3/2} \approx 457$ and $2p_{1/2} \approx 463$ eV) (Figure 3b). Thus, the surface of nitridated shells consists of Ti–O, Ti–N, and Ti–N–O chemical bonding states. These different bonding states of Ti in the nitridated shells can be explained by the thermal decomposition of NH_3 to H_2 and N_2 at high temperature (>550 °C).[14] The decomposed hydrogen gas can play a role in partially reducing TiO_2,

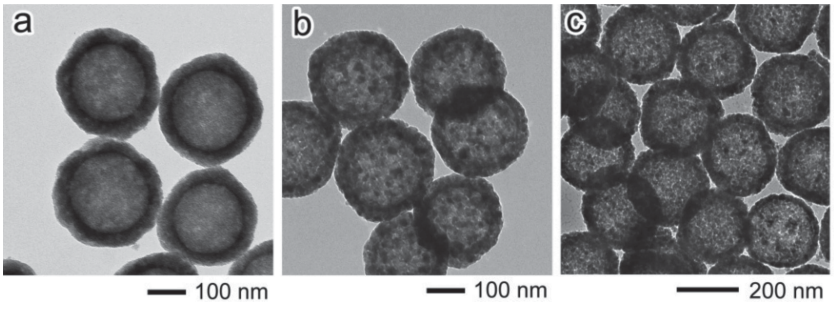

Figure 1. TEM images of a) sol–gel derived amorphous TiO_2 shells, b) crystalline TiO_2 shells after calcination in air at 800 °C, c) nitridated shells treated at 900 °C under a NH_3 atmosphere.

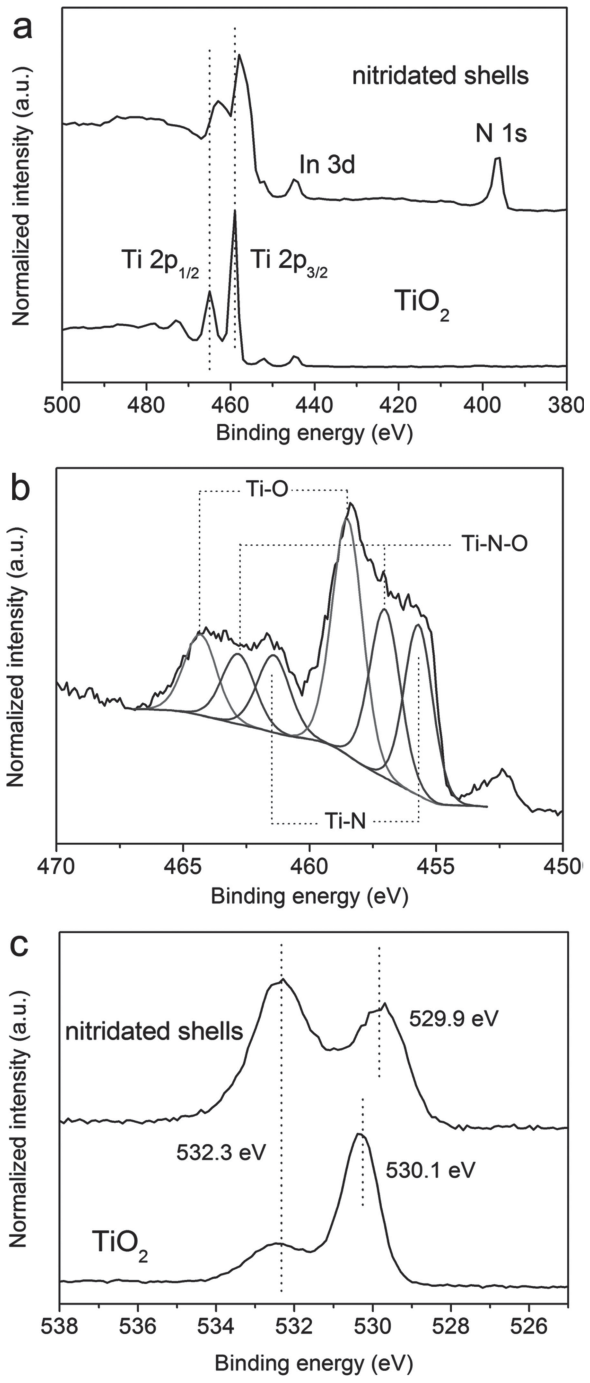

Figure 3. a) XPS spectra of hollow TiO_2 sphere calcined at 800 °C and nitridated shell treated at 900 °C under NH_3 (20 mL min^{-1}) and Ar (80 mL min^{-1}). b) Deconvoluted XPS spectra showing the split Ti bands of nitridated sample. c) Normalized O 1s core level XPS spectra of TiO_2 and nitridated sample.

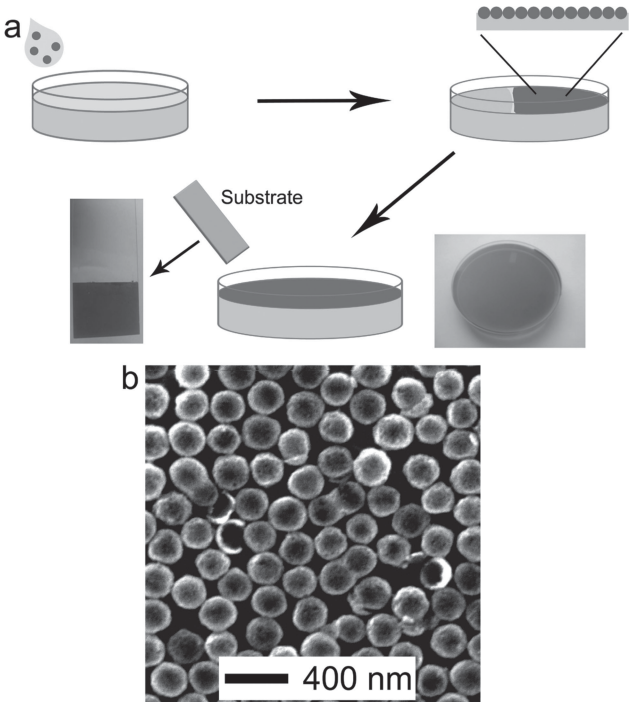

Figure 4. a) Schematic illustration of the manufacturing process for the assembled monolayer of hollow nitridated shells for electrochemical electrodes. The digital images show the assembled nitridated shells on a water surface (right) and the transferred film on glass (left). b) SEM image of the hollow nitridated shells transferred to a silicon substrate.

which facilitates the penetration of nitrogen and the formation of oxygen vacancies in the TiO_2 crystal structure. Both hollow TiO_2 and nitridated shell samples exhibit the peak for Ti–O–Ti bonding at binding energies of ≈530 eV, as shown in Figure 3c, suggesting the existence of oxide even after nitridation.[17] Additionally, the peak of higher energy than Ti–O–Ti bonding corresponds to Ti–OH bonding and the relative intensity of this peak in the nitridated titania sample increased after nitridation, which is indicative of the increased presence of hydroxyl groups on the surface of nitridated titania compared to bare TiO_2.[18]

Figure 4a schematically shows the fabrication process for an assembled monolayer film of hollow nitridated shells. The well-dispersed nitridated shells in 1-butanol were dropped on the water surface in a container. Due to the high surface tension of water, nitridated shells suspended in 1-butanol starts to spread on the water surface and finally forms a robust film, which is not ruptured by any fluctuation.[19] To transfer the film, the desired substrate was immersed in water and scooped up through the film of nitridated shells on top of the water. Repetition of this simple process can produce a multi-layered nitridated shell film. The digital images in Figure 4a show an assembled monolayer of nitridated shells on water (right) and the film after being transferred onto glass (left). Figure 4b shows a scanning electron microscopy (SEM) image of the obtained film of nitridated shells, confirming the monolayer structure.

Electrochemical impedance studies were conducted to investigate the effect of nitridation on the electrical properties of the hollow TiO_2 shells. **Figure 5** shows the Mott–Schottky plots based on capacitances that were obtained from the electrochemical impedance at 10 kHz in the dark in the potential range of 0 to 0.7 V. Hollow TiO_2 shells show a clear positive slope, a typical characteristic of an *n*-type semiconductor. The Mott-Schottky equation gives the carrier density of a semiconductor as follows:

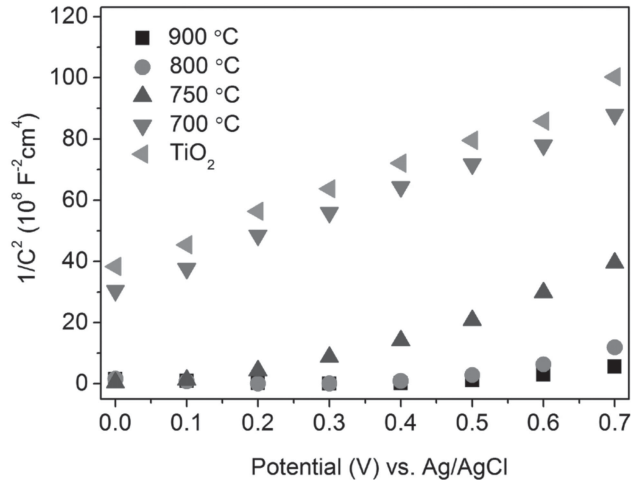

Figure 5. Mott-Schottky plots of hollow TiO_2 sphere calcined at 800 °C and hollow shells nitridated at different temperatures.

$$N_d = \frac{2}{e_0 \varepsilon \varepsilon_0} \left[\frac{d\left(\frac{1}{C^2}\right)}{dV} \right]^{-1} \quad (1)$$

where N_d, e_0, ε, and ε_0 are donor density, electron charge, relative permittivity, and permittivity of vacuum, respectively. The carrier density of hollow TiO_2 spheres is determined to be 5.8×10^{20} cm^{-3} by employing the relative permittivity of TiO_2 (30 for anatase).[20] A quantitative comparison between hollow TiO_2 spheres and nitridated shells is difficult due to the invalidity of the relative permittivity of titanium nitride because of its metallic character. Nevertheless, a qualitative comparison of the carrier densities of hollow TiO_2 spheres and nitridated shells reveals that the slope of the Mott-Schottky plot for nitridated titania is much lower than that of TiO_2, indicating higher carrier densities for nitridated titania samples. The carrier density increases for samples nitridated at higher temperatures. The increased carrier density can be attributed to the electronic character of nitridated titania since titanium nitride has a very high electronic conductivity (~10^6 S m^{-1}, bulk).

To investigate the electrochemical properties of the assembled nitridated shell film, electrochemical measurements were conducted in 1 M Na_2SO_4 aqueous solution with a three-electrode system containing Pt wire and Ag/AgCl as a counter and reference electrode, respectively. Indium tin oxide (ITO) glass substrate was used as a working electrode by scooping up the assembled nitridated shell film, followed by drying in air at 90 °C for 30 min. The working electrode was the as-prepared TiO_2 or nitridated shell film (three layers) with an electrode area of 1 cm^2. **Figure 6** shows typical cyclic voltammetric curves (CV) and galvanostatic charge-discharge curves of the assembled film of nitridated shell . TiO_2 and nitridated titania samples display no pseudocapacitive oxidation/reduction peaks, which only show quasi-rectangular CV curves (Figure S3, Supporting Information). In comparison to the TiO_2 film, the nitridated titania sample exhibits better capacitive properties. The enclosed area of the CV curve in nitridated titania sample is about 45 times larger than that of the TiO_2 sample (**Figure 7**a).

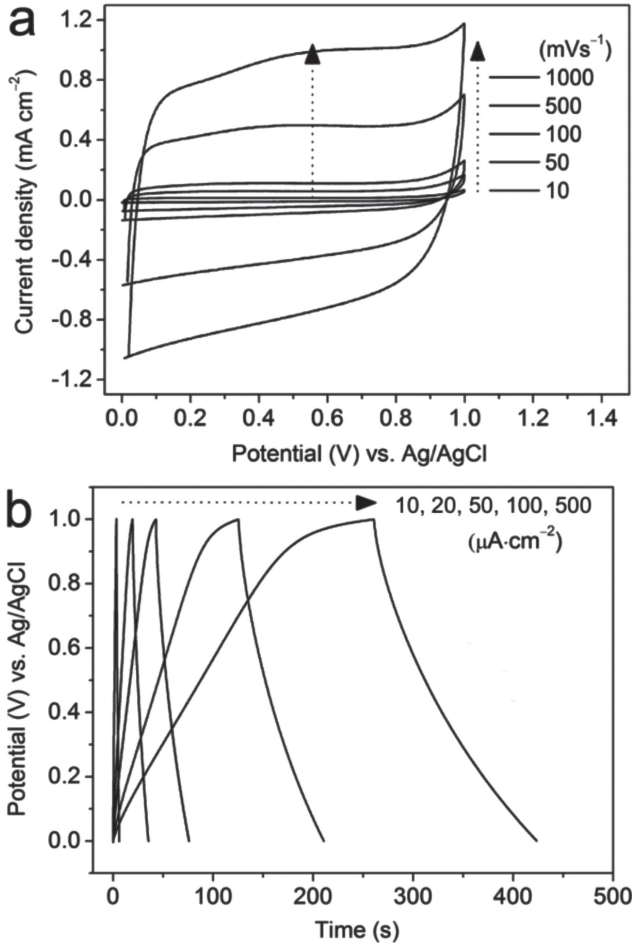

Figure 6. a) CV curves of the assembled nitridated shell film collected at various scan rates in the range of potentials between 0 and 1 V. b) Galvanostatic charge–discharge curves of the assembled film of hollow shells nitridated at 900 °C at various current densities.

The areal capacitances of hollow TiO_2 sphere and nitridated shell electrodes were calculated as a function of scan rate (Figure 7b). The areal capacitance obtained from galvanostatic charge–discharge measurements can be calculated by the following equation:

$$C = \frac{I \times \Delta t}{\Delta V \times A} \quad (2)$$

where I, Δt, ΔV, and A are the constant discharging current, time, potential window, and electrode area, respectively. The areal capacitance of the nitridated shell film electrode is 2.48 and 1.91 mF cm^{-2} at scan rates of 10 and 100 mV s^{-1}, respectively, which are 181 and 258 times higher than those of the hollow TiO_2 shell film electrode (0.0137 and 0.0074 mF cm^{-2}). Previously reported areal capacitances of TiO_2 nanotube arrays and TiO_2 nanoparticles are less than 1 mF cm^{-2}.[6] The improved electrochemical performance of the nitridated shell film electrode can be attributed to the enhancement of the electronic properties upon nitridation. The nitridated shell film offers an electronically conducting framework and a fast charge separation network desirable for electrochemical energy

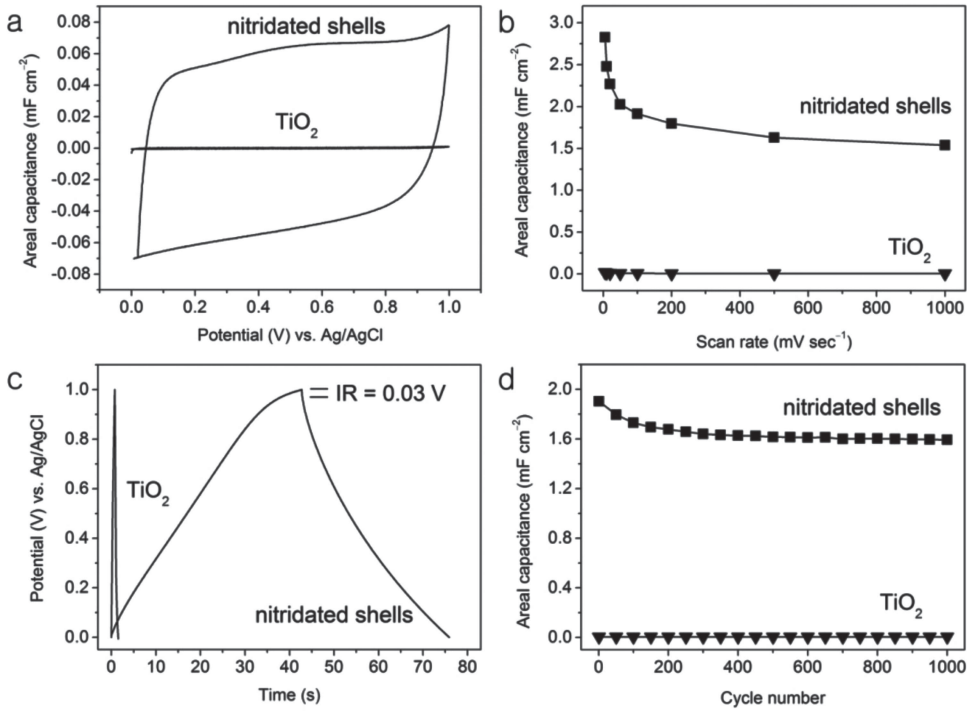

Figure 7. a) CV curves of three-layer films made from hollow TiO_2 and nitridated shells on ITO glass at a scan rate of 50 mV s^{-1}. b) Areal capacitances of the assembled films of hollow TiO_2 and nitridated shells as a function of scan rate. c) Galvanostatic charge-discharge curves of TiO_2 and nitridated titania at a current density of 50 μA cm^{-2}. d) Cycling performance of TiO_2 and nitridated titania supercapacitors at a scan rate of 200 mV $^{-1}$ for 1000 cycles.

storage. Furthermore, the nitridated shell film shows a better rate capacitance than the TiO_2 shell film. The areal capacitance of the nitridated shell sample drops from 2.48 to 1.54 mF cm^{-2} with retention of 62% when the scan rate increases from 10 to 1000 mV/s. In contrast, the bare TiO_2 film electrode maintains only 39 % of the initial capacitance. As the rate capability is dependent on the rate of ion diffusion (mass transport) and the conductivity of the electrode, the improved retention rate of the nitridated shell sample is attributed to the enhanced electrical conductivity of the electrode due to the formation of TiN since the sample morphologies are both hollow structures, which implies a similar ion diffusion rate. Figure 7c shows the galvanostatic charge-discharge curves of both shell samples collected at a current density of 50 μA cm^{-2}. The curve of the nitridated titania electrode is substantially prolonged compared to the TiO_2 electrode, indicating a good capacitive behavior. In addition, it has a small IR drop (0.03 V), confirming the low internal resistance of the nitridated titania film. As suggested in Figure 7d, the nitridated shell electrode shows good cycling stability up to 1000 cycles at a scan rate of 200 mV s^{-1}, where CV curves show small current reduction (11.3% decay) during the cycling (Figure S4, Supporting Information).

As mentioned above, the electrochemical performance of the film electrode of nitridated shells is closely related to its electrical conductivity (carrier density). As the carrier density of the nitridated shells was observed to depend on the nitridation conditions, we further studied the effect of the nitridation temperature on the electrochemical performance. As seen in **Figure 8**a, the capacitive current density in CV curves of the nitridated titania electrode increases when the nitridation temperature is raised from 700 to 900 °C. As expected from electrical conductivity, the sample nitridated at 900 °C yields the highest current density in CV curves while the one nitridated at 700 °C shows no difference in its capacitive CV curve compared to the original TiO_2 sample. Notably, there is no obvious enhancement between samples nitridated at 800 and 900 °C while a large increase in areal capacitance was obtained between TiO_2 sphere samples nitridated at 700 and 800 °C. Thus, it can be inferred that the conducting pathway is completed at around 800 °C, followed by the saturation of electrochemical performance. Moreover, areal capacitances calculated from discharge curves (Figure 8c) show that the nitridated shell film electrode at 900 °C achieved the highest values at a current density range between 5 and 1000 μA cm^{-2}, which is consistent with the result from CV curves. The areal capacitances of the sample nitridated at 700 °C were measured only up to 50 μA cm^{-2} due to poor charge-discharge performance.

An additional advantage of the assembly process is the potential to improve the electrochemical properties of the material through multi-layer stacking. Figure 8d shows that the areal capacitances of the 800 and 900 °C nitridated titania samples calculated from the integration of CV curves at a scan rate of 50 mV s^{-1} were found to scale linearly with the number of layers. By fabricating a simple multi-stacked film electrode, the areal capacitance of the sample nitridated at 900 °C can be increased up to 7 mF cm^{-2} at a scan rate of 50 mV s^{-1}. On the other hand, there was no increase in the areal capacitances of the bare TiO_2 and the sample nitridated at 700 °C. It should

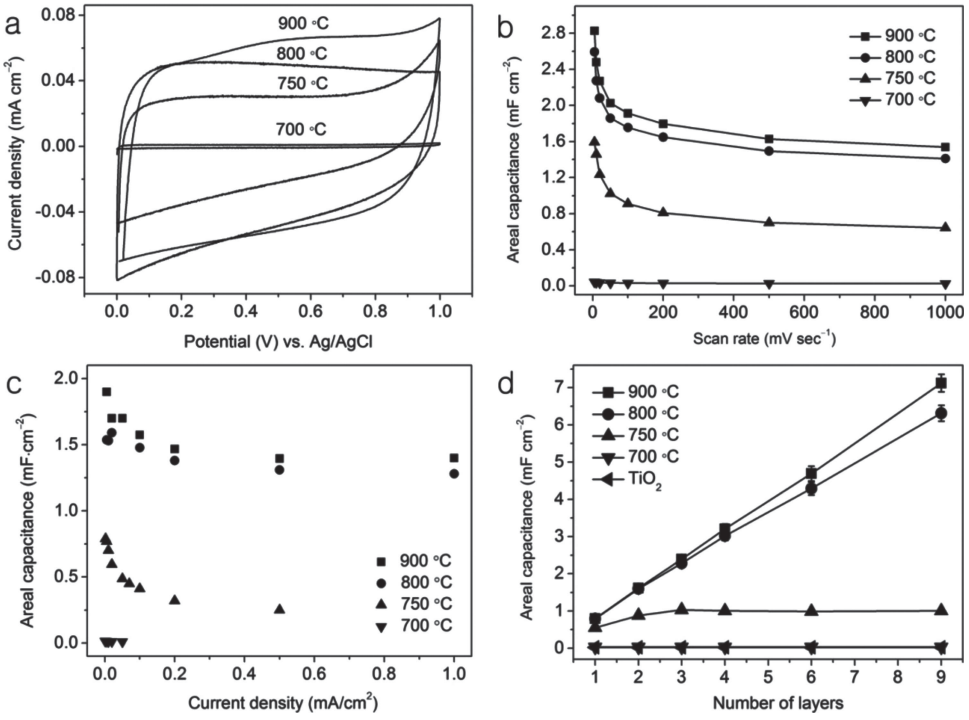

Figure 8. a) CV curves of assembled films of hollow nitridated shell samples with different nitridation temperatures collected at a scan rate of 50 mV s^{-1}. b) Areal capacitances of the nitridated shell samples as a function of scan rate. c) Areal capacitances of the nitridated shell samples measured as a function of current density. Due to poor charge-discharge performance, the areal capacitance of nitridated titania treated at 700 °C was only measured up to 0.05 mA cm^{-2}. d) Areal capacitances of the hollow TiO_2 sphere and nitridated shell samples as a function of number of layers by calculating based on CV curves at a scan rate 50 mV s^{-1}.

be noted that the nitridated titania electrode treated at 750 °C shows a small linear increase up to three layers, followed by a saturation of electrochemical performance. The poor electrochemical performance of the samples nitridated below 800 °C and bare TiO_2 reconfirms that the electrical conductivity must be high enough to create a pathway for charge to separate from the surface of active materials and move to the current collector.

The assembled film of nitridated shells is also a potential framework for constructing three dimensional conducting networks when decorated with electrochemically active materials. As a proof-of-concept study, we selected MnO_2 as the electroactive component due to its high theoretical capacitance and low electronic conductivity. Despite the promising pseudocapacitive properties of MnO_2, the low electrical conductivity (~10^{-5} S m^{-1}) limits its use without an additional conducting component. The synthesis of a MnO_2/nitridated titania (also MnO_2/TiO_2) composite electrode was accomplished by deposition of MnO_2 through the reaction of an aqueous $KMnO_4$ solution with ethanol (Figures S1,S2, Supporting Information).[21] MnO_2 deposition on the nitridated shell film electrode was confirmed by XPS study, which clearly shows the characteristic peaks for binding energy corresponding to Mn $2p_{3/2}$ and Mn $2p_{1/2}$ (Figure S7, Supporting Information). **Figure 9**a shows the areal capacitances of MnO_2-coated samples as a function of scan rate. The areal capacitance of the MnO_2/nitridated sample gained a large enhancement, which is ≈240 times higher than the MnO_2/TiO_2 sample at a scan rate of 50 mV s^{-1}. The areal capacitance at scan rates from 5 to 1000 mV s^{-1} was increased by about 4.5 times compared to the samples before MnO_2 deposition. This result demonstrates that the nitridated shell film can be a good support for supercapacitors with electroactive materials.

It is generally understood that a hollow structure is superior to a solid one due to its shorter mass diffusion and transport resistance, presuming the surface area is the same. To investigate the advantage of hollow nitridated shells for supercapacitor applications, we conducted a comparison study versus porous nitridated titania spheres, which were produced by nitridating porous anatase TiO_2 spheres under NH_3 at 900 °C. The synthesis of mesoporous anatase spheres involves hydrolysis of silica precursor in a solution of colloidal TiO_2, followed by calcination of the composite to crystallize the amorphous TiO_2 into anatase structure and removal of the silica through chemical etching.[22] As shown in the inset of Figure 9a, the spheres remain porous after nitridation at 900 °C. Nitrogen adsorption and desorption tests revealed that the hollow shells and porous nitridated titania spheres have surface areas of 46 and 62 m^2 g^{-1}, respectively, with similar pore sizes (≈1.0 nm) (Figure S8, Supporting Information). As expected, the capacitive current density of porous nitridated titania sphere film was slightly higher than that of the hollow nitridated shell sample mainly due to the larger surface area of porous sample. However, the MnO_2/nitridated titania (hollow) electrode exhibited a higher areal capacitance than the MnO_2/nitridated titania (porous) sample. The capacitance increase through the deposition of MnO_2 on the porous nitridated titania sphere film is lower than that for the hollow nitridated shell sample, by the

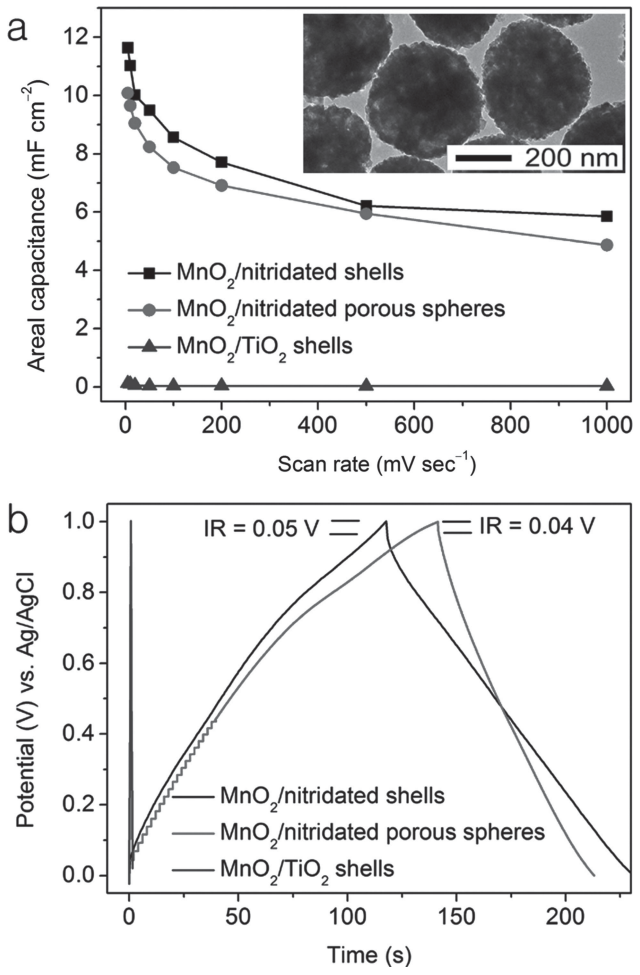

Figure 9. a) Areal capacitances of MnO_2-coated TiO_2 and nitridated titania (porous and hollow) samples as a function of scan rate. The inset is a TEM image of the porous nitridated titania spheres. b) Galvanostatic charge-discharge curves of TiO_2 and nitridated samples at a current density of 50 μA cm^{-2}.

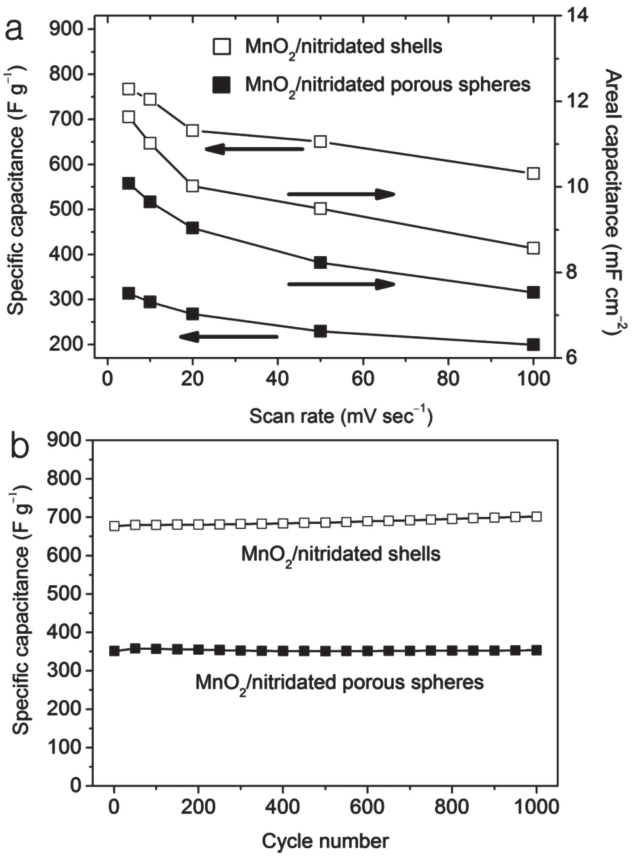

Figure 10. a) Gravimetric capacitances and areal capacitances of nitridated porous spheres and nitridated hollow shells coated with MnO_2 as a function of scan rate. b) Cycling performance of the samples at a scan rate of 200 mV s^{-1} for 1000 cycles.

increments of 2.2- and 4.7-fold for the porous and hollow samples, respectively. After deposition of MnO_2 on the nitridated titania film, the CV curves of MnO_2/nitridated titania composite exhibit a rectangular shape, with clear oxidation/reduction peaks indicating pseudo-capacitive behavior from the activity of MnO_2 (Figure S10, Supporting Information). Galvanostatic charge-discharge tests also confirmed the better performance of the hollow sample over the porous one (Figure 9b), as determined by the prolonged time for the hollow sample at a current density of 50 μA cm^{-2}. From the discharging curves of MnO_2-coated porous and hollow nitridated titania samples, the calculated areal capacitances are 3.58 and 5.68 mF cm^{-2}, respectively, which is consistent with the trend of the CV curves.

To better understand the electrochemical activity of the deposited MnO_2 on the nitridated titania films (porous and hollow), we compared the gravimetric capacitances by measuring the loading amount of MnO_2 with ICP-AES (inductively coupled plasma-atomic emission spectroscopy). The specific capacitance was calculated as follows:

$$C_{MnO_2} = \frac{Q_{MnO_2/Tin-QTin}}{\Delta V \times m_{MnO_2}} \quad (3)$$

where Q, ΔV, and m are the average charge during the CV process, potential window, and loading mass, respectively. The loading mass of MnO_2 in the nitridated porous titania sphere film was larger than that in the nitridated shell film due to the larger surface area of the nitridated porous titania sphere film (19.6 and 11.4 μg for porous sphere and hollow shell samples, respectively). **Figure 10**a shows the specific capacitances of both samples as a function of scan rate together with the corresponding areal capacitances for comparison. Based on the measured specific capacitances, the MnO_2/nitridated shell sample achieved better electrochemical properties by about a 2.5-fold larger capacitance through scan rates from 5 to 100 mV s^{-1}. It should be noted that the specific capacitances of the MnO_2/nitridated shells dropped with the time of MnO_2 deposition, which verifies that only a thin layer of MnO_2 on the surface of nitridated shells can be utilized as an electrochemically active area (Figure S13, Supporting Information). Cycling performance is one of the most important factors in determining supercapacitor properties. Cycling stability tests of MnO_2/nitridated shells (porous and hollow) samples were conducted at a scan rate of 200 mV s^{-1} (Figure 10b). Both MnO_2/nitridated titania

electrodes maintained their initial capacitances up to 1000 cycles, which reveals a good long-term cyclic performance.

3. Conclusion

We have demonstrated that nitridated hollow shells can be produced via a simple nitridation process and that facile 2D self-assembly of these shells enables the creation of a robust monolayer film, which can be exploited as a supercapacitor electrode through a binder-free approach. The increased electrical conductivity due to the formation of TiN and functionalization with hydroxyl groups on the surface of the nitridated shells greatly enhance the electrochemical performance compared to a porous TiO_2 sphere electrode. In addition, the areal capacitance of the nitridated shell electrode can be tuned by making a multi-layered film electrode, which shows a linear increase between the number of layers and the areal capacitance. Furthermore, we have shown that the nitridated shell film can be an excellent scaffold to support other pseudocapacitive materials to produce composite structures with greatly improved electrochemical performance, due to the high electrical conductivity of nitride phase and the short diffusion path of the hollow structures.

4. Experimental Section

Synthesis of Hollow TiO_2 Spheres: Hollow TiO_2 spheres were obtained by following a process previously reported by our group.[15a] In a typical synthesis, spherical colloidal silica templates were first prepared via the Stöber process. Tetraethyl orthosilicate (TEOS, 3.44 mL) was added into a mixture of water (13.2 mL), aqueous ammonium hydroxide (28%, 2.48 mL), and ethanol (92 mL), with a reaction time of 4 h. For the conformal coating of TiO_2, hydroxypropyl cellulose (HPC, 0.3 g) was dissolved in ethanol (80 mL) and water (0.48 mL) and to this solution the washed silica colloid suspended in ethanol (20 mL) was added and stirred for 30 min. Next, titanium n-butoxide (4 mL) in ethanol (18 mL) was injected into the above solution by syringe pump at a pumping rate of 0.5 mL min^{-1}, followed by heating to 85 °C for 100 min, resulting in the formation of SiO_2@TiO_2 spheres. Then the washed SiO_2@TiO_2 sample was redispersed in 80 ml H_2O, mixed with an aqueous NaOH solution (2.5 M, 5 mL), followed by shaking the mixture for 6 h. The resulting hollow shells were redispersed in 40 ml H_2O, mixed with an aqueous HCl solution (0.1 M, 10 mL) to protonate the titanate species.[15b] The product was finally washed, dried, and calcined in air at 800 °C for 3 h to obtain anatase TiO_2 hollow spheres.

Nitridation of TiO_2 Shells: The as-prepared hollow TiO_2 spheres were placed in a quartz tube furnace under Ar and NH_3 at flow rates of 80 and 20 mL min^{-1}, respectively. The temperature was ramped at 2 °C min^{-1} and maintained at the designated temperature (700, 750, 800, and 900 °C) for 2 h. After being cooled to room temperature, nitridated TiO_2 shells were obtained as deep blue/ black powders.

Characterization: The morphology of the samples were investigated with scanning electron microscopy (SEM, XL 30) and transmission electron microscopy (TEM, Philips Tecnai 12, 200 kV). Powder XRD patterns were obtained with a Bruker D8 Advance Powder X-ray diffractometer using Cu Kα radiation. The mass of MnO_2 deposited on the nitridated film was measured by Inductive Coupled Plasma-Atomic Emission Spectroscopy (ICP-AES, PerkinElmer, Optima 2000 DV). X-ray photoelectron spectroscopy (XPS) characterization was performed by using a Kratos AXIS ULTRA^{DLD} XPS system equipped with an Al Kα monochromated X-ray source and a 165-nm electron energy hemispherical analyzer. The binding energy was calibrated for each sample by referencing the C 1s peak to 284.6 eV. The nitrogen adsorption isotherm was studied by using a nitrogen physisorption instrument (Quantachrome NOVA 4200e) at 77 K.

Preparation of Electrode and Electrochemical Tests: The electrode was prepared by exploiting an assembled film of spheres on a water surface, followed by transferring the film onto a solid substrate. TiO_2 and nitridated shells were dispersed in 1-butanol by ultrasonication. This suspension was dropped on a water surface in a Petri dish with a pipette until a robust film was formed. The film was then scooped up by an ITO glass substrate repeatedly to make a multi-layer film. For the deposition of MnO_2 on the nitridated film, the nitridated film was placed in a vial containing $KMnO_4$ solution (10 mL, 0.1 M) under magnetic stirring. Then, ethanol (5 mL) was dropped into the vial for different amounts of time (2–30 min, reaction time) and the film was washed with D.I. water, followed by drying in an oven for 30 min. All the electrochemical data were obtained by using a three-layer film electrode by repeating the transfer process three times. The electrochemical properties of the samples were measured using cyclic voltammetry (CV) and galvanostatic charge-discharge measurements in a conventional three-electrode system with a potentiostat (VersaSTAT 4, Princeton Applied Research). The working electrode was the as-prepared TiO_2 or nitridated shell film (three layers) with an electrode area of 1 cm^2. The reference and counter electrodes were Ag/AgCl (1 M KCl) and a platinum wire, respectively. Mott-Schottky plots were obtained at 10 000 Hz. The cyclic performance of the electrodes was investigated by CV measurements at a scan rate of 200 mV s^{-1}. All the electrochemical tests were performed in 1 M Na_2SO_4 aqueous solution at room temperature after purging with nitrogen gas for 20 min.

Supporting Information

Supporting Information is available from the Wiley Online Library or from the author. It includes additional electrochemical data of TiO_2 and shells nitridated at different temperatures, TEM image of the nitridated porous titania spheres, nitrogen adsorption and desorption isotherms of hollow and porous nitridated samples, and XPS spectrum showing the Mn 2p levels of the MnO_2/nitridated film.

Acknowledgements

This project was financially supported by the Winston Chung Global Energy Center at UCR. Yin also thanks the Research Corporation for Science Advancement for the Cottrell Scholar Award and DuPont for the Young Professor Grant.

Received: May 21, 2013
Revised: August 1, 2013
Published online: September 19, 2013

[1] a) G. Pfaff, P. Reynders, *Chem. Rev.* **1999**, *99*, 1963; b) A. Salvador, M. C. Pascual-Martí, J. R. Adell, A. Requeni, J. G. March, *J. Pharm. Biomed. Anal.* **2000**, *22*, 301; c) D. B. Strukov, G. S. Snider, D. R. Stewart, R. S. Williams, *Nature* **2008**, *453*, 80; d) M. Grätzel, *Nature* **2001**, *414*, 338.

[2] a) F. Zuo, L. Wang, T. Wu, Z. Zhang, D. Borchardt, P. Feng, *J. Am. Chem. Soc.* **2010**, *132*, 11856; b) X. Chen, S. S. Mao, *Chem. Rev.* **2007**, *107*, 2891.

[3] a) K. Wang, M. Wei, M. A. Morris, H. Zhou, J. D. Holmes, *Adv. Mater.* **2007**, *19*, 3016; b) D. Wang, D. Choi, J. Li, Z. Yang, Z. Nie, R. Kou, D. Hu, C. Wang, L. V. Saraf, J. Zhang, I. A. Aksay, J. Liu, *ACS Nano* **2009**, *3*, 907.

[4] a) T. Brousse, R. Marchand, P.-L. Taberna, P. Simon, *J. Power Sources* **2006**, *158*, 571; b) Z. Yang, D. Choi, S. Kerisit, K. M. Rosso,

D. Wang, J. Zhang, G. Graff, J. Liu, *J. Power Sources* **2009**, *192*, 588.
[5] T. Brezesinski, J. Wang, J. Polleux, B. Dunn, S. H. Tolbert, *J. Am. Chem. Soc.* **2009**, *131*, 1802–1809.
[6] a) M. S. Kim, T.-W. Lee, J. H. Park, *J. Electrochem. Soc.* **2009**, *156*, A584; b) M. Salari, K. Konstantinov, H. K. Liu, *J. Mater. Chem.* **2011**, *21*, 5128; c) Y. Xie, D. Fu, *Mater. Res. Bull.* **2010**, *45*, 628.
[7] a) J. Wang, J. Polleux, J. Lim, B. Dunn, *J. Phys. Chem. C* **2007**, *111*, 14925; b) F. Fabregat-Santiago, E. M. Barea, J. Bisquert, G. K. Mor, K. Shankar, C. A. Grimes, *J. Am. Chem. Soc.* **2008**, *130*, 11312.
[8] X. Lu, G. Wang, T. Zhai, M. Yu, J. Gan, Y. Tong, Y. Li, *Nano Lett.* **2012**, *12*, 1690.
[9] Y. Xie, L. Zhou, C. Huang, H. Huang, J. Lu, *Electrochim. Acta* **2008**, *53*, 3643.
[10] S. A. Sherrill, J. Duay, Z. Gui, P. Banerjee, G. W. Rubloff, S. B. Lee, *Phys. Chem. Chem. Phys.* **2011**, *13*, 15221.
[11] S. Dong, X. Chen, L. Gu, X. Zhou, L. Li, Z. Liu, P. Han, H. Xu, J. Yao, H. Wang, X. Zhang, C. Shang, G. Cui, L. Chen, *Energy Environ. Sci.* **2011**, *4*, 3502.
[12] S. Dong, X. Chen, L. Gu, X. Zhou, H. Xu, H. Wang, Z. Liu, P. Han, J. Yao, L. Wang, G. Cui, L. Chen, *ACS Appl. Mater. Interfaces* **2010**, *3*, 93.
[13] D. Choi, P. N. Kumta, *J. Electrochem. Soc.* **2006**, *153*, A2298.
[14] D. A. Cooper, E. B. Ljungstroem, *Energy Fuels* **1988**, *2*, 716.
[15] a) J. B. Joo, Q. Zhang, M. Dahl, I. Lee, J. Goebl, F. Zaera, Y. Yin, *Energy Environ. Sci.* **2012**, *5*, 6321; b) J. B. Joo, I. Lee, M. Dahl, G. D. Moon, F. Zaera, Y. Yin, *Adv. Funct. Mater.* **2013**, DOI: 10.1002/adfm.201300255.
[16] S. Pétigny, H. Mostéfa-Sba, B. Domenichini, E. Lesniewska, A. Steinbrunn, S. Bourgeois, *Surf. Sci.* **1998**, *410*, 250.
[17] X. Chen, L. Liu, P. Y. Yu, S. S. Mao, *Science* **2011**, *331*, 746.
[18] a) E. McCafferty, J. P. Wightman, *Surf. Interface Anal.* **1998**, *26*, 549; b) X. Lu, D. Zheng, T. Zhai, Z. Liu, Y. Huang, S. Xie, Y. Tong, *Energy Environ. Sci.* **2011**, *4*, 2915.
[19] G. D. Moon, T. I. Lee, B. Kim, G. Chae, J. Kim, S. Kim, J.-M. Myoung, U. Jeong, *ACS Nano* **2011**, *5*, 8600.
[20] S. K. Kim, G. W. Hwang, W.-D. Kim, C. S. Hwang, *Electrochem. Solid-State Lett.* **2006**, *9*, F5.
[21] J. Bae, M. K. Song, Y. J. Park, J. M. Kim, M. Liu, Z. L. Wang, *Angew. Chem., Int. Ed.* **2011**, *50*, 1683.
[22] M. Dahl, S. Dang, J. Bong Joo, Q. Zhang, Y. Yin, *CrystEngComm* **2012**, *14*, 7680.